AIP Journal of Applied Physics

Structural and optical analysis of GaAsP/GaP core-shell nanowires

P. K. Mohseni, A. D. Rodrigues, J. C. Galzerani, Y. A. Pusep, and R. R. LaPierre

Citation: Journal of Applied Physics **106**, 124306 (2009); doi: 10.1063/1.3269724
View online: http://dx.doi.org/10.1063/1.3269724
View Table of Contents: http://scitation.aip.org/content/aip/journal/jap/106/12?ver=pdfcov
Published by the AIP Publishing

Articles you may be interested in
Incorporation of Be dopant in GaAs core and core–shell nanowires by molecular beam epitaxy
J. Vac. Sci. Technol. B **34**, 02L114 (2016); 10.1116/1.4943600

Self-catalyzed growth of dilute nitride GaAs/GaAsSbN/GaAs core-shell nanowires by molecular beam epitaxy
Appl. Phys. Lett. **107**, 103111 (2015); 10.1063/1.4930887

Electrical transport and optical model of GaAs-AlInP core-shell nanowires
J. Appl. Phys. **111**, 094319 (2012); 10.1063/1.4716011

Structural and optical properties of InGaN–GaN nanowire heterostructures grown by molecular beam epitaxy
J. Appl. Phys. **109**, 014309 (2011); 10.1063/1.3530634

Structural and optical properties of Zn 0.9 Mn 0.1 O / ZnO core-shell nanowires designed by pulsed laser deposition
J. Appl. Phys. **106**, 093501 (2009); 10.1063/1.3253572

Reuse of AIP Publishing content is subject to the terms at: https://publishing.aip.org/authors/rights-and-permissions. Download to IP: 129.21.154.238 On: Fri, 15 Apr 2016 18:57:24

Structural and optical analysis of GaAsP/GaP core-shell nanowires

P. K. Mohseni,[1] A. D. Rodrigues,[2] J. C. Galzerani,[2] Y. A. Pusep,[3] and R. R. LaPierre[1,a)]
[1]*Department of Engineering Physics, Centre for Emerging Device Technologies, McMaster University, Hamilton, Ontario L8S 4L7, Canada*
[2]*Departamento de Fisica, Universidade Federal de São Carlos, CP676, 13565-905, São Carlos, São Paulo, Brazil*
[3]*Instituto de Fisica de São Carlos, Universidade de São Paulo, 13560-970 São Carlos, São Paulo, Brazil*

(Received 6 August 2009; accepted 4 November 2009; published online 18 December 2009)

The structural and optical properties of GaAsP/GaP core-shell nanowires grown by gas source molecular beam epitaxy were investigated by transmission electron microscopy, Raman spectroscopy, photoluminescence (PL), and magneto-PL. The effects of surface depletion and compositional variations in the ternary alloy manifested as a redshift in GaAsP PL upon surface passivation, and a decrease in redshift in PL in the presence of a magnetic field due to spatial confinement of carriers. © *2009 American Institute of Physics*. [doi:10.1063/1.3269724]

I. INTRODUCTION

An emerging class of optoelectronic and photonic devices is being realized by semiconductor nanowires (NWs).[1] The pseudo-one-dimensionality of NWs offers a unique opportunity to control size-dependent and structure-dependent material properties for novel device functionalities. Of particular interest is the use of core-shell NW architectures, composed of ternary III-V compound semiconductor alloys, which provide further freedom to tune the material bandgap including the optical frequency range.[2–5] Encapsulation of core NW segments by higher bandgap shell layers provides passivation of surface states, where nonradiative recombination transitions are prevalent, as well as the confinement of charge carriers within the core segment.

Core-shell NW growth has been demonstrated through a variety of means. The most common epitaxial approaches involve metal-organic vapor phase epitaxy[6,7] and molecular beam epitaxy (MBE).[8,9] The most widely reported mechanism for NW assembly is the so called vapor-liquid-solid (VLS) mechanism.[10–12] During VLS growth, gas-phase adatoms impinge on, or diffuse toward, liquid-phase metal nanoparticles [typically Au, but also Ga (Ref. 13) and Cu (Ref. 14)] resulting in a metal-semiconductor alloy. Supersaturation of the Au alloy leads to island nucleation at a triple-phase-point,[15] proceeded by solid-phase semiconductor epilayer formation at the interface between the liquid alloy seed and the underlying substrate. VLS growth is continued, and, thus, a NW is grown, as long as sufficiently high supersaturation conditions are sustained.

Optoelectronic device applications based on the employment of III-V NWs as the active medium have recently been demonstrated, including lasers,[16] photovoltaic cells,[17] and single photon sources.[18] Nonetheless, integration of NW-based applications within mainstream markets is hindered by numerous fundamental roadblocks, one of which involves a more complete understanding of the role of surface passivation and confinement effects.

In this work, we report on the structural and optical properties of GaP/GaAsP core-shell NWs grown according to the VLS mechanism. We show that radial and axial layers are distinctly self-arranged within a single segment of a ternary semiconductor NW, resulting in increased P incorporation near the center of the NW. The effect of this compositional variance and the influence of a passivating GaP shell on the optically active GaAsP regions are investigated through Raman scattering, photoluminescence (PL), and magneto-PL (M-PL) spectroscopy.

II. EXPERIMENTAL DETAILS

NWs were grown on (111)-oriented n-type Si substrates. Pregrowth surface processing of the Si substrates was initiated with a 20 min ultraviolet ozone treatment and subsequent wet-etching of the surface oxide in a 10:1 diluted buffered HF solution. Seeds for the NW growth were achieved by electron-beam evaporation of Au with thickness of 10 or 40 Å as measured by a quartz crystal monitor. All substrates were stored under high vacuum (10^{-8} Torr) to inhibit surface contamination until transfer to the growth chamber.

NW growth was performed in a gas source MBE (GS-MBE) system, where group III monomers were supplied from a heated solid elemental effusion cell and group V dimers from a hydride gas cracker operating at 950 °C. The P_2 flux was initiated at 350 °C as the substrate temperature was ramped from room temperature to the NW growth temperature. Upon stabilization at the growth temperature, the As_2 flux was initiated. At the substrate temperature of 520 °C, growth was initiated by opening the shutter of the Ga effusion cell, 60 s after the initiation of the As_2 flux.

Three NW samples of different sizes and structures were grown and investigated in the current study, henceforth referred to as samples A, B, and C. Details of the NW growth are provided in Table I. Sample A NWs were grown using a 10 Å Au film and composed of a single segment of $GaAs_{1-x}P_x$, with an As/P flux ratio adjusted to yield a nominal composition of $x=0.4$, based on previous calibrations of thin films grown on GaAs (100) substrates. The growth duration of sample A NWs was 30 min. Sample B NWs were

a)Electronic mail: lapierr@mcmaster.ca.

 © 2009 American Institute of Physics

Reuse of AIP Publishing content is subject to the terms at: https://publishing.aip.org/authors/rights-and-permissions. Download to IP: 129.21.154.238 On: Fri, 15 Apr 2016 18:57:24

TABLE I. Description and dimensions of NW samples A–C.

NW sample	Au film thickness (Å)	Growth sequence	NW height (μm)	NW FWHL diameter (nm)
A	10	30 min GaAsP	3.75	53
B	10	30 min GaAsP +10 min GaP	5.50	96
C	40	30 min GaAsP	3.50	101

grown in an identical manner to that of sample A with the addition of a single, stoichiometric GaP segment, grown for a duration of 10 min, and serving as a passivation layer to the GaAsP core. Thus, the sample B NWs were grown to inherently contain GaAsP/GaP core-shell heterostructures. Sample C NWs were grown under identical conditions as sample A except a 40 Å Au film was employed in sample C rather than the 10 Å Au film used in sample A. All growths were conducted at a V/III flux ratio of 1.5. The group III effusion cell temperature was stabilized to yield a nominal planar growth rate of 1 μm h^{-1}. The growths were terminated by closing the shutter of the Ga effusion cell, and the sample was gradually cooled down from the growth temperature under a P_2 overpressure. Pictorial representation of the three NW samples based on our structural analysis is shown in Fig. 1 as will be discussed further below.

Structural and compositional analysis of the NW samples was performed after growth. A JEOL JSM-7000 scanning electron microscope (SEM) was employed in the cross-sectional analysis of as-grown NW samples, particularly in the determination of average NW heights. Single NW specimens, ultrasonically removed in solution from the Si substrates and deposited on holey carbon-coated copper grids, were examined with a Philips CM12 transmission electron microscope (TEM). In addition, compositional analysis was performed in various positions along the NW length by embedding NWs in an epoxy resin (vinyl cyclohexene dioxide)[19] cured at 70 °C, followed by the removal of lateral lamellae with average thicknesses of roughly 80–100 nm, using an ultramicrotomy procedure, at a slicing angle of approximately 5°. Lamellae were subsequently placed on TEM grids and sputter coated with a thin film of carbon (roughly 5 nm) to further reduce superficial electron-beam-induced damage. The lamellae were examined by high angle annular dark field (HAADF) characterization and energy dispersive x-ray spectrometry (EDXS) using a JEOL 2010F high-resolution TEM.

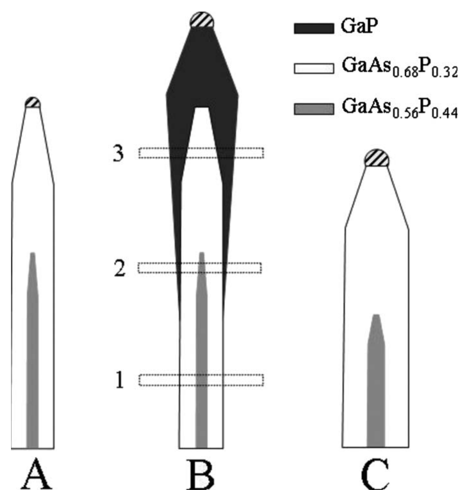

FIG. 1. Pictorial representation of sample A, B, and C NW structures. The NWs are not drawn to scale. White and light gray segments represent As-rich and P-rich GaAsP layers, respectively. The dark gray segment of the sample B NW signifies the GaP layer. Dotted boxes, labeled 1, 2, and 3, correspond to the regions of interest on the ultramicrotomed lamellae presented in Figs. 4 and 5. The striped segments at the NW tips represent the Au seed nanoparticles.

Raman scattering, PL, and M-PL were performed to study the lattice vibrations and electron excitations of samples A–C. The investigation of the lattice vibrations (phonons) by Raman scattering allowed a structural characterization of the NWs, while PL provided information about the electronic structure of the NWs. Raman scattering was collected from the surface of the samples at a temperature T=10 K in the backscattering configuration with an Instruments S.A. T64000 triple grating spectrometer supplied with a liquid nitrogen-cooled charge coupled device detector. The PL measurements were carried out at T=1.6 K with an Ocean Optics Inc. HR2000 high-resolution spectrometer in an Oxford Instruments optical cryostat with a superconducting magnet with magnetic field of 10 T oriented parallel to the NWs. The 5145 Å line of an Ar^+ laser was used for excitation in Raman and PL measurements.

III. RESULTS AND DISCUSSION

A. Electron microscopy analysis

The average NW heights were determined in cross-sectional SEM images by measuring the distance between the planar surface and the top of the Au seeds at the NW tips. Representative cross-sectional SEM images of all NW samples are shown in Fig. 2. The NW heights were measured to be approximately 3.75, 5.5, and 3.5 μm for samples A, B, and C NWs, respectively. The SEM images revealed that the NWs were tapered near their tips, while also exhibiting reverse tapering near their bases, as shown in the inset of Fig. 2(b) and depicted in Fig. 1(b). Therefore, the diameters of NWs was quantified via their average full width at half length (FWHL) as measured in TEM from a population of 100 sonicated NWs per sample. The average FWHLs of the NWs were determined to be 53 ± 11 nm for sample A, 96 ± 9 nm for sample B, and 101 ± 20 nm for sample C NWs. Figure 3 shows a comparison of the normalized

Reuse of AIP Publishing content is subject to the terms at: https://publishing.aip.org/authors/rights-and-permissions. Download to IP: 129.21.154.238 On: Fri, 15 Apr 2016 18:57:24

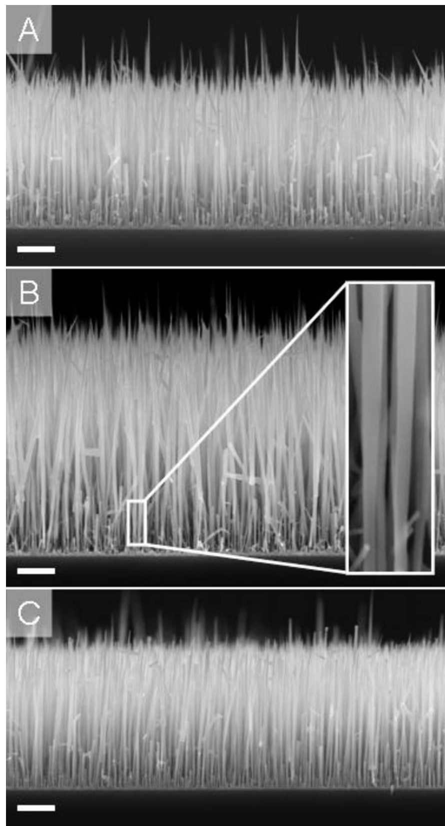

FIG. 2. Cross-sectional SEM images of as-grown NW samples (a) A, (b) B, and (c) C. The highlighted region and inset in (b) further illustrates the reverse tapering phenomenon, due to shadowing effects. All scale bars represent a 1 μm length.

FWHL distributions for each NW sample, fit to a Gaussian distribution, wherein the above uncertainty values represent one standard deviation. The above results are summarized in Table I.

The larger diameter of sample B compared to sample A NWs is attributed to the presence of the passivating GaP shell in sample B but not A. In contrast, the disparity between average FWHL values observed for samples A and sample C NWs is the consequence of the thicker Au film employed in the growth of sample C NWs. The thicker Au

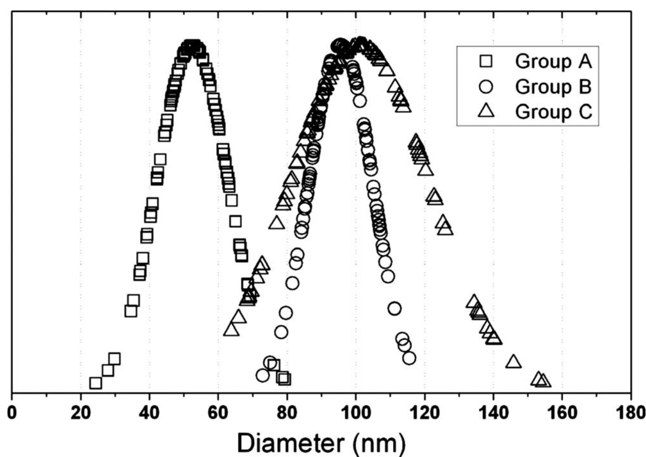

FIG. 3. FWHL NW diameters of samples A, B, and C, fit to a Gaussian distribution. The profiles represent sample sets of 100 single NWs.

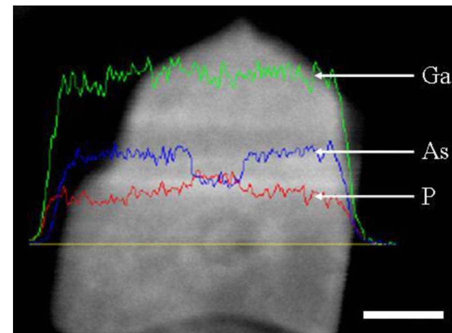

FIG. 4. (Color online) HAADF image showing the cross-section of a single sample B NW near its base (corresponding to box 1 in Fig. 1). EDXS linescans, representative of elemental Ga (green), As (blue), and P (red), are superimposed. The decrease in the As profile and increase in P profile observed near the center corresponds to the region of dark contrast, and demonstrates the presence of a P-rich region near the NW center. The scale bar represents a 20 nm length.

film results in larger Au nanoparticles upon annealing. The length of NWs is inversely proportional to the Au seed particle diameter due to a simple material conservation principle.[11,20] Larger Au nanoparticles therefore result in the growth of thicker, yet shorter, structures.

We previously reported the ternary alloy composition of NWs, grown under identical conditions as the present study, to be $GaAs_{0.67}P_{0.33}$ along the longitudinal center of the NW, based on a cylindrical approximation technique involving EDXS mapping and HAADF imaging of individual NWs.[2] In this study, a more accurate determination of the structure and composition of the NWs were achieved by examining lamellae cut from the sample B NWs. Sections removed from the NW bases, midsection, and tips (represented in Fig. 1 as boxes 1, 2, and 3, respectively) were probed in EDXS experiments to determine the elemental distributions across the NW diameter at various lengths along the NW. Figure 4 shows a HAADF image of a lamella removed from the base region of a sample B NW (box 1 in Fig. 1) with superimposed EDXS linescans, indicative of the elemental concentrations of Ga (green), As (blue), and P (red). While the elemental counts of Ga are observed to be constant across the NW diameter, the As and P counts, in contrast, are noted to deviate from a homogenous profile within the center. In the NW center, the elemental concentration of As atoms declines, whereas the concentration of P atoms rises. Thus, a P-rich region is evident near the radial center of the GaAsP NW. EDXS mapping in several NWs indicated a region with composition of $GaAs_{0.56}P_{0.44}$ near the NW center (depicted as the gray region in Fig. 1) with a surrounding composition of $GaAs_{0.68}P_{0.32}$ (depicted as the white region in Fig. 1). The GaP passivating layer was notably absent from the base of the NWs which can be explained by shadowing effects [see also the inset of Fig. 2(b)]. The GaP shell is initiated after the GaAsP segment is completed. At this point, the NWs have already reached a certain critical height where shadowing from neighboring NWs could limit the direct impingement near each NW base.[7,21] As a result, the GaP shell is absent near the base of the NWs as depicted in Fig. 1.

Next, a cross-sectional segment removed from the central region of a sample B NW (box 2 in Fig. 1) was examined

Reuse of AIP Publishing content is subject to the terms at: https://publishing.aip.org/authors/rights-and-permissions. Download to IP: 129.21.154.238 On: Fri, 15 Apr 2016 18:57:24

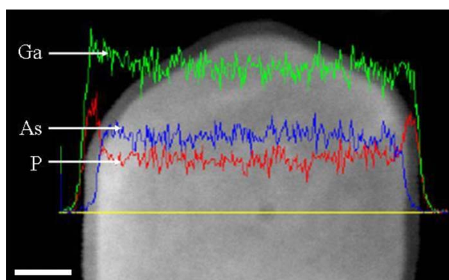

FIG. 5. (Color online) Cross-sectional HAADF image and superimposed EDXS linescans showing elemental counts of Ga (green), As (blue), and P (red), obtained from the axial midsection of a single sample B NW (corresponding to box 2 in Fig. 1). A passivating GaP shell is seen as an outer disk of dark contrast. A central spot of dark contrast shows the location of a small P-rich region near the NW center, which is unresolved by the EDXS linescan. The scale bar represents a 20 nm length.

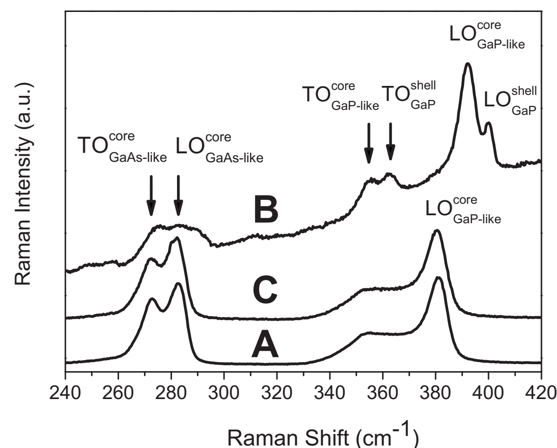

FIG. 6. Raman spectra of the samples A, B, and C measured at T=10 K. The spectra have been shifted vertically for clarity.

as shown in Fig. 5. Here, EDXS measurements indicated a homogenous composition of $GaAs_{0.68}P_{0.32}$ in close agreement with our previous cylindrical approximation method.[2] Although no notable variation in the As/P ratio could be spatially resolved by EDXS, a centrally localized region of dark contrast was resolved in the HAADF image, associated with the presence of a small P-enriched inner region within the GaAsP layer. Toward the circumference, the dramatic decrease in As counts and sharp increase in P counts is characteristic of the presence of the passivating GaP layer, which is also evident by the darker contrast along the NW circumference.

Similar EDXS scans obtained from the tips of sample B NWs (not shown) demonstrated a GaAsP core diameter reduction and an increase in the thickness of the GaP shell as depicted by box 3 in Fig. 1. Previous investigations into the nature of MBE-grown core-multishell NW heterostructures, involving the same material samples, has led us to conclude that the aforementioned effect is a result of the tapered or "pencil-shaped" morphology of NWs grown under similar conditions as depicted in Fig. 1.[2,22] EDXS mapping indicated a homogeneous composition of $GaAs_{0.68}P_{0.32}$ in this tip region of the NW, identical to the composition of the NW midsection and outer regions of the NW base.

Based on the above EDXS analysis, P-enrichment occurs in the center of the base region of the NWs with a composition of approximately $GaAs_{0.56}P_{0.44}$. A composition of $GaAs_{0.68}P_{0.32}$ was measured throughout other regions of the NW. Initially, the main contribution to NW growth is adatom impingement on the substrate surrounding each NW, followed by adatom diffusion to the Au particle resulting in axial NW growth or direct nucleation on the NW sidewalls resulting in radial growth. A previous thermodynamic model for the incorporation of group V species in InGaAsP films during GS-MBE growth[23] indicated the preferential incorporation of As compared to P, suggesting a longer diffusion length before incorporation of P_2 compared to As_2 on the substrate surface. Therefore, the species with longer diffusion length (P_2) would be expected to contribute more to axial growth of the NW that would lead to P-enrichment of the NW center as we observed, as compared to the species with shorter diffusion length (As_2) that would contribute more to radial growth of the NW. When the NW becomes sufficiently long, the contribution to axial growth due to adatom diffusion from the substrate diminishes and the main contribution to NW growth then changes to direct impingement near the Au seed particle at the top of the NW. In this case, differences in As_2 and P_2 diffusion on the NW sidewalls and the Au seed particle may become less significant, which limits the P-enrichment near the base of the NWs.

B. Raman scattering analysis

Raman spectra of samples A–C are shown in Fig. 6. The GaAs-like and GaP-like transverse optical (TO) and longitudinal optical (LO) phonons were clearly observed in the single segment GaAsP NWs (samples A and C). Moreover, considerable Raman scattering was observed in the single segment NWs (samples A and C) in the interval between the TO and LO GaP-like phonons. Such Raman scattering was not found in the encapsulated NW (sample B) where the surface was passivated. Therefore, it is likely due to the surface modes present in the NWs with open surfaces.[24,25] The relative frequency positions (ν_{LO}^{GaP}, ν_{LO}^{GaAs}) and integral intensities (I_{LO}^{GaP}, I_{LO}^{GaAs}) of the GaP-like and GaAs-like LO phonons in samples A and C allow a determination of the P concentration of the $GaAs_{1-x}P_x$ alloy according to the formulas[26]

$$\nu_{LO}^{GaP}(x) = 350.1 + 72.2x - 20.0x^2, \quad (1)$$

$$\nu_{LO}^{GaAs}(x) = 291.1 - 25.5x, \quad (2)$$

$$x = \frac{I_{LO}^{GaP}}{I_{LO}^{GaP} + I_{LO}^{GaAs}}. \quad (3)$$

The frequencies and the integral intensities of the GaP-like and GaAs-like LO phonons were obtained from fits of the experimental Raman spectra by Gaussian lines. The integral intensities yield $x \approx 0.48$, while the positions of the GaAs-like and GaP-like LO phonon frequencies (interpolated to room temperature) give $x \approx 0.43$ and $x \approx 0.42$, respectively. In comparison, a composition $x \approx 0.44$ was obtained from EDXS analysis for the center of the NW base and $x \approx 0.32$ elsewhere. Raman cannot distinguish between

Reuse of AIP Publishing content is subject to the terms at: https://publishing.aip.org/authors/rights-and-permissions. Download to IP: 129.21.154.238 On: Fri, 15 Apr 2016 18:57:24

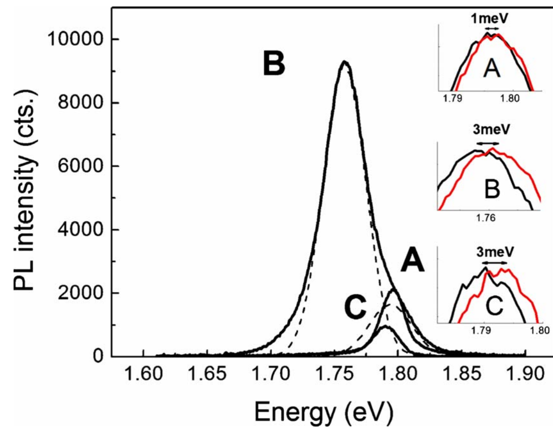

FIG. 7. (Color online) PL spectra of the samples A, B, and C measured at T=1.6 K. Insets show the comparisons between the PL measured close to the peak positions without the magnetic field (black lines) and in the magnetic field B=10 T (red lines). The dashed lines show two contributions to the PL emission in sample B.

contributions from different parts of the NW. Instead, the Raman lines will consist of the weighted average contributions of the entire NW. In addition, compositional determination by Raman is complicated by scattering effects within the NWs.[27]

The Raman data obtained in the encapsulated NWs (sample B) clearly demonstrate the effect of the core-shell misfit accommodation. The GaP-like LO phonon line is considerably blueshifted with respect to the corresponding lines in the single segment NWs (samples A and C). Moreover, the LO phonon line of the GaP shell is redshifted with respect to the frequency of the bulk GaP LO phonon (404 cm^{-1}). This is a manifestation of the stressed GaAsP core and the tensile GaP shell, which is expected from the difference in corresponding lattice constants.

C. Photoluminescence analysis

The PL spectra of the NWs are depicted in Fig. 7. The single segment NWs (samples A and C) emitted narrow PL lines with peak positions near 1.8 eV. The slightly different PL peak positions of samples A and C (a difference of about 6 meV) is likely caused by the effects of spatial confinement. The TEM analysis indicated an average NW diameter (FWHL) of 53 nm for sample A and 101 nm for sample C (see Table I and Fig. 3). The large diameter of the sample C NWs does not result in a significant quantization of the electron energy. However, for sample A, a confinement energy of about 1.5 meV was calculated by the envelope function approximation using the parameters from Ref. 28. The difference between the experiment (6 meV) and the calculation (1.5 meV) may be explained by assuming a smaller effective "electronic" diameter of sample A, caused by spatial confinement due to surface depletion, as discussed further below.

The effects of the spatial confinement were further measured by magneto-PL measurements. The magnetic field does not influence the electron energy when the NW diameter $D_{NW} < L_B$, where $L_B = \sqrt{\hbar / eB}$ is the magnetic length. In the magnetic field of B=10 T the magnetic length is about 10 nm. In such a magnetic field one expects a blueshift in the PL measured in the $GaAs_{1-x}P_x$ NW samples of about 7 meV (calculated as the energy shift in the lowest Landau level). The PL peak intensities in the magnetic field B=10 T are compared with the PL intensities measured without the field in the insets of Fig. 7. Only a very small (about 1 meV) blueshift was found in sample A with the nominal diameter of 53 nm. An absence of the anticipated blueshift in sample A indicates a considerably smaller effective electronic diameter, which results in determination of the electron energy mainly due to spatial confinement. Larger blueshifts in the PL lines (about 3 meV) measured in the magnetic field of 10 T were observed in samples B and C indicating less spatial confinement compared to sample A. When the magnetic length is much larger than the effective electronic NW diameter ($L_B > D_{NW}$) the electron energy is completely determined by the NW size quantization. In such a case no variation in the PL energy with the magnetic field is expected. In the opposite limit ($L_B < D_{NW}$) the magnetic field is responsible for the electron energy quantization. In the bulk GaAsP, in the magnetic field B=10 T ($L_B \approx 10$ nm), the magnetic field induced PL blueshift of about 7 meV is expected. In samples B and C we measured the blueshifts of 3 meV, which means that in these samples the magnetic field considerably influences the electron energy, which, together with the spatial confinement, determines the electron energy. Accordingly, D_{NW} is on the order of but somewhat larger than $L_B \approx 10$ nm in samples B and C. In sample A, a much smaller shift was observed (about 1 meV) in the magnetic field. Hence, the effective NW diameter, $D_{eff} < L_B \approx 10$ nm in sample A, which is consistent with the previously presented zero-field blueshift in the PL peak position of sample A compared to C.

The most striking effect is the significant redshift and the substantial increase in intensity of the PL found in the encapsulated core-shell sample B compared to A and C. A similar increase in the PL intensity was found in the core-shell InGaP/GaAs NWs in Ref. 29. The increase in PL emission upon encapsulation of the NWs is due to passivation of the surface states which cause nonradiative recombination of the excited electrons. Another striking observation is the redshift in the PL in the passivated NWs of sample B, while a blueshift is expected due to the shell strain.[29]

The Franz–Keldysh effect,[30,31] caused by the built-in surface electric field and observed recently in InP,[32] also cannot explain our observed redshift in the PL emission. Passivation of surface states responsible for the built-in electric field eliminates the effect of the surface band bending. Therefore, a blueshift in the PL emission, opposite our observed redshift, is expected in the encapsulated NWs.

Based on the extensive structural analysis of the NWs presented earlier, a model is developed to account for the observed modification of the PL emission. We suppose that the P-enrichment of the central GaAsP segment found through the EDXS analysis plays a crucial role in the detected redshift in the PL emission. The model radial distribution of the electron potential assumed in the passivated sample B is shown in Fig. 8. The P-enrichment of the central part of the core-shell GaAsP/GaP NWs causes the radial gradient of the electron gap energy shown in Fig. 8(a). Electrons

Reuse of AIP Publishing content is subject to the terms at: https://publishing.aip.org/authors/rights-and-permissions. Download to IP: 129.21.154.238 On: Fri, 15 Apr 2016 18:57:24

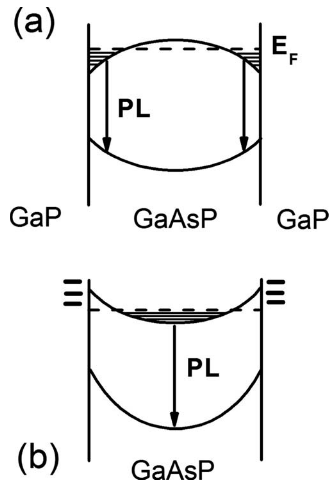

FIG. 8. Sketch of the radial distribution of the electron gap in the core-shell GaAsP/GaP (a) and in the single segment GaAsP (b) NWs. The electron transitions active in the PL are shown by the vertical arrows.

are confined in the narrow ranges of the NWs close to the GaAsP/GaP interface. This circular range occupied by the electrons is responsible for the PL emission. The band bending due to surface states of the single segment GaAsP (samples A and C) produces the built-in electric field, which depletes the electron states and shifts the range where the electrons are confined to the inner part of the NW with the larger gap (higher P content in the center of the NW base). The corresponding radial gap variation is depicted in Fig. 8(b). Therefore, the energy of the core-shell NWs decreases as compared to the single segment NWs. This model also accounts for the smaller effective electronic diameters of the NWs mentioned above.

The surface depletion effects can be estimated using the well-known relation for a semi-infinite slab

$$qD_s = \sqrt{2\kappa\varepsilon_o N\psi_s}, \tag{4}$$

where D_s is the surface charge density, κ is the dielectric constant, ε_o is the vacuum permittivity (8.85×10^{-12} F cm^{-1}), N is the doping level, and ψ_s is the surface potential (surface band bending). We assume an unintentional n-type doping level in the NW identical to that determined by Hall effect measurements in nominally undoped thin films (n-type with $N\sim10^{15}$ cm^{-3}). κ is taken as 12.53, which is the dielectric constant of the $GaAs_{0.56}P_{0.44}$ shell, calculated as the compositional weighted average of the GaAs and GaP dielectric constants. The band bending due to the compositional difference between the center and edge of the GaAsP segment is approximated as the PL peak energy difference of 30 meV between samples B and C. Using Eq. (4), a potential due to surface states may exceed the band bending due to composition if $D_s > 2\times10^{11}$ cm^{-2}.

Finally, a somewhat broader and asymmetrical PL line was observed in sample B as compared to samples A and C. The fit of the PL line using Gaussian profiles clearly demonstrates the presence of two distinct lines: a weak one centered at the energy 1.8 eV and a stronger one at 1.76 eV. The weak PL line probably has the same origin as the PL emission from samples A and C, namely, this is caused by the emission from the bottom, core segment of the NWs that remained unpassivated due to the shadowing effect. The strong PL line is due to the core/shell upper segment as discussed above.

IV. CONCLUSIONS

An extensive analysis consisting of structural and spectroscopic experimental techniques was performed in GaAsP NWs. The radial variation in the P composition detected through EDXS mapping measurements was shown to drastically influence the PL emission. The combined effects of the radial P distribution and of the built-in electric field cause the different locations of the PL active ranges in areas with different bandgaps. This results in the considerable change in the PL emission energy.

ACKNOWLEDGMENTS

Financial support from Brazilian agencies FAPESP, CNPq, the Natural Sciences and Engineering Research Council of Canada, the Ontario Centres of Excellence, and the Canadian Institute for Photonic Innovations is gratefully acknowledged.

[1]Y. Li, F. Qian, J. Xiang, and C. M. Lieber, Mater. Today **9**, 18 (2006).
[2]P. K. Mohseni, C. Maunders, G. A. Botton, and R. R. LaPierre, Nanotechnology **18**, 445304 (2007).
[3]C. Chen, S. Shehata, C. Fradin, R. R. LaPierre, C. Couteau, and G. Weihs, Nano Lett. **7**, 2584 (2007).
[4]E. D. Minot, F. Kelkensberg, M. van Kouwen, J. A. van Dam, L. P. Kouwenhoven, V. Zwiller, M. T. Borgstrom, O. Wunnicke, M. A. Verheijen, and E. P. A. M. Bakkers, Nano Lett. **7**, 367 (2007).
[5]D. L. Dheeraj, G. Patriarche, L. Largeau, H. L. Zhou, A. T. J. van Helvoort, F. Glas, J. C. Harmand, B. O. Fimland, and H. Weman, Nanotechnology **19**, 275605 (2008).
[6]K. Tomioka, J. Motohisa, S. Hara, and T. Fukui, Nano Lett. **8**, 3475 (2008).
[7]K. A. Dick, K. Deppert, L. Samuelson, L. R. Wallenberg, and F. M. Ross, Nano Lett. **8**, 4087 (2008).
[8]P. K. Mohseni, G. Lawson, C. Couteau, G. Weihs, A. Adronov, and R. R. LaPierre, Nano Lett. **8**, 4075 (2008).
[9]J. C. Harmand, G. Patriarche, G. Pere-Laperne, M. N. Merat-Combes, L. Travers, and F. Glas, Appl. Phys. Lett. **87**, 203101 (2005).
[10]R. S. Wagner and W. C. Ellis, Appl. Phys. Lett. **4**, 89 (1964).
[11]V. G. Dubrovskii, N. V. Sibirev, G. E. Cirlin, J. C. Harmand, and V. M. Ustinov, Phys. Rev. E **73**, 021603 (2006).
[12]H. J. Fan, P. Werner, and M. Zacharias, Small **2**, 700 (2006).
[13]C. Colombo, D. Spirkoska, M. Frimmer, G. Abstreiter, and A. Fontcuberta i Morral, Phys. Rev. B **77**, 155326 (2008).
[14]O. Demichel, F. Oehler, P. Noe, V. Calvo, N. Pauc, P. Gentile, T. Baron, D. Peyrade, and N. Magnea, Appl. Phys. Lett. **93**, 213104 (2008).
[15]F. Glas, J. C. Harmand, and G. Patriarche, Phys. Rev. Lett. **99**, 146101 (2007).
[16]B. Hua, J. Motohisa, Y. Kobayashi, S. Hara, and T. Fukui, Nano Lett. **9**, 112 (2009).
[17]J. A. Czaban, D. A. Thompson, and R. R. LaPierre, Nano Lett. **9**, 148 (2009).
[18]M. T. Borgström, V. Zwiller, E. Muller, and A. Imamoglu, Nano Lett. **5**, 1439 (2005).
[19]A. R. Spurr, J. Ultrastruct. Res. **26**, 31 (1969).
[20]P. K. Mohseni and R. R. LaPierre, Nanotechnology **20**, 025610 (2009).
[21]M. C. Plante and R. R. LaPierre, J. Cryst. Growth **286**, 394 (2006).
[22]M. C. Plante and R. R. LaPierre, Nanotechnology **19**, 495603 (2008).
[23]R. R. LaPierre, B. J. Robonson, and D. A. Thompson, J. Appl. Phys. **79**, 3021 (1996).
[24]G. D. Mahan, R. Cupta, Q. Xiong, C. K. Adu, and P. C. Eklund, Phys. Rev. B **68**, 073402 (2003).

Reuse of AIP Publishing content is subject to the terms at: https://publishing.aip.org/authors/rights-and-permissions. Download to IP: 129.21.154.238 On: Fri, 15 Apr 2016 18:57:24

[25]D. Spirkoska, G. Abstreiter, and A. Fontcuberta i Morral, Nanotechnology **19**, 435704 (2008).
[26]M.-E. Pistol and X. Liu, Phys. Rev. B **45**, 4312 (1992).
[27]O. L. Muskens, S. L. Diedenhofen, B. C. Kaas, R. E. Algra, E. P. A. M. Bakkers, J. G. Rivas, and A. Lagendijk, Nano Lett. **9**, 930 (2009).
[28]I. Vurgaftman, J. R. Meyer, and L. R. Ram-Mohan, J. Appl. Phys. **89**, 5815 (2001).
[29]N. Sköld, L. S. Karlsson, M. W. Larsson, M.-E. Pistol, W. Seifert, J. Trägårdh, and L. Samuelson, Nano Lett. **5**, 1943 (2005).
[30]W. Franz, Z. Naturforsch. A **13a**, 484 (1958).
[31]L. V. Keldysh, J. Exp. Theor. Phys. **33**, 994 (1957).
[32]M. H. M. van Weert, O. Wunnicke, A. L. Roest, T. J. Eijkemans, A. Yu Silov, J. E. M. Haverkort, G. W. 't Hooft, and E. P. A. M. Bakkers, Appl. Phys. Lett. **88**, 043109 (2006).

Reuse of AIP Publishing content is subject to the terms at: https://publishing.aip.org/authors/rights-and-permissions. Download to IP: 129.21.154.238 On: Fri, 15 Apr 2016 18:57:24